Band narrowing and Mott localization in isotropically superstrained graphene

L. Craco,[1] S. S. Carara,[1] and S. Leoni[2]
[1]*Instituto de Física, Universidade Federal de Mato Grosso, 78060-900, Cuiabá, Mato Grosso, Brazil*
[2]*School of Chemistry, Cardiff University, Cardiff CF10 3AT, United Kingdom*
(Received 10 August 2016; published 26 October 2016)

We explore the effect of multiorbital electron-electron interactions in a two-dimensional monolayer made of elemental carbon. Using density functional dynamical mean-field theory (DFDMFT), we show that the interplay between one-particle band narrowing and sizable on-site interactions naturally stabilizes the Mott insulating state in isotropically superstrained graphene. Our theory is expected to be a key step to understanding both the ability of graphene to afford large strain deformations and the changes in electronic degrees of freedom of p-band Coulomb interacting electrons for the next generation of flexible electronics made of semiconductive graphene.

DOI: 10.1103/PhysRevB.94.165168

I. INTRODUCTION

Graphene is a two-dimensional monolayer of carbon atoms arranged in a hexagonal honeycomb lattice structure (see Fig. 1). Its electronic properties at low energies are mostly governed by elementary excitations created around the Fermi surface [1]. These elementary excitations are known to be massless Dirac fermions with a linear spectrum. In recent years, graphene has attracted the attention of the wider scientific community due to a range of physical properties, suggesting its application in fields as diverse as photonics, sensor technology, and spintronics [2]. More precisely, graphene and its derivatives are expected to form the next generation of (radio frequency) transistors [3], flexible electronics [4,5], spintronics [6], and nanoelectronic devices [7], as well as electrochemical, biological, and gas sensors [2,8]. However, the semimetallic nature of graphene with a Dirac-like spectrum near the Fermi energy E_F and finite conductivity values [9] seems to prevent its application as the host material for the next generation of flexible electronic devices [5] and stretchable transparent electrodes [4]. Hence, what is needed to have full working devices made of graphene is to find promising directions for band gap engineering of graphene [10].

Recently, several experimental and theoretical proposals have been made to open an energy gap in the electronic spectra of graphene. Experimentally, it has been found that an energy gap can be induced in epitaxial graphene on a SiC substrate via strong graphene-substrate interaction [10]. A semiconducting regime in epitaxial graphene can also be developed by suitable molecular doping [11]. Theoretical studies have predicted similar routes for tuning graphene's band gap. An interesting proposal is, for example, that a small band gap opens up in the band structure of graphene when water or ammonia molecules adhere to its surface [12]. A similar effect is also observed when gold nanoparticles are deposited on graphene's surface [13]. An alternative approach of producing a charge gap in the spectrum of graphene is to deposit it on top of a lattice-matched hexagonal boron nitride substrate [14]. Moreover, the potential to tune novel physical properties, including band gap tuning [15], of graphene by applying mechanical strain has been explored in recent years both experimentally [4,16–18] and theoretically [19,20]. Theoretically, at the one-particle level strain can turn semimetal graphene metallic [20,21] (see also our results below). Importantly, several experiments have been performed to explore the physical properties of graphene when its hexagonal lattice is stretched out of its equilibrium [16,17]. Uniaxial strain can be induced by bending the substrates on which graphene is elongated [15]. Graphene on top of a SiX ($X = O_2$, C) surface [18] also experiences a moderate strain due to surface corrugations or lattice mismatch. Presently, graphene can be stretched to 30% [4]; however, it is worth noting that carbon-nanotube films with a serpentine morphology can be stretched 170% once before failure [22], meaning that pristine graphene might have higher sheer elasticity and stretchability than hitherto probed. In fact, experiments performed on graphene/poly(dimethylsiloxane) composites [23] seem to corroborate our prediction by showing that these flexible conductors can support strains higher than 50% before they start to break. Thus, motivated by this and other studies on stretchable patterned graphene systems [8] as well as by an experimental study [17] establishing graphene as the strongest material ever seen in nature, we carried out first-principles generalized gradient approximation plus dynamical mean-field theory (GGA+DMFT) [24] calculations to investigate changes in the electronic properties of isotropically superstrained graphene. We show that following incorporation of on-site Coulomb correlations via GGA+DMFT, an energy gap naturally opens up in graphene with nearly 52% stretching [20]. We thus expect that under controlled, albeit extreme, strain conditions the interplay between electron-electron interactions [25] and lattice strain will naturally induce Mott localization, i.e., the formation of a gapped excitation spectrum at low energies in superstrained graphene.

The proximity to a Mott-Hubbard metal-insulator transition point [26] (Mottness) is a clear manifestation of dynamical many-body effects in correlated electrons. Historically, the Mott transition was considered to occur as a function of the expansion of the lattice constant L. In Mott's picture [27], a first-order transition from an insulator to a metallic state takes place at a critical value $L = L_c$. For $L > L_c$ a cubic crystalline array of one-electron atoms should be in a charge-insulating state, whereas for $L < L_c$, one should have a metal. The charge gap at the Mott transition jumps discontinuously from a finite value to zero. Mott's original idea was to tune the ratio U/W between the on-site Coulomb interaction U and the one-particle bandwidth W (i.e., the kinetic energy of the electrons), which defines the phase boundary between the

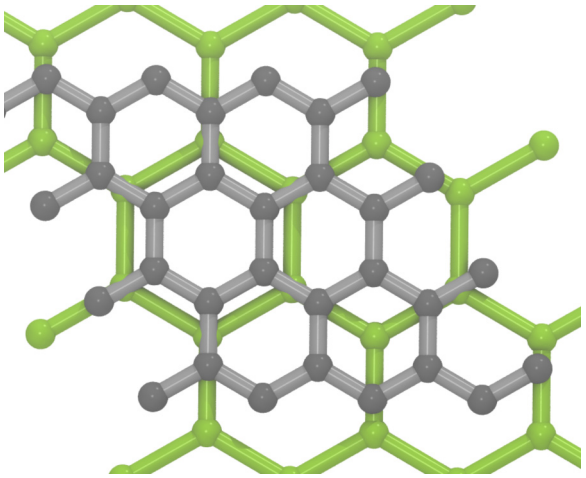

FIG. 1. Crystal structure of natural ($L = 0.24669$ nm) and superstrained ($L = 0.3759$ nm) graphene, with L being the lattice constant of the system.

metallic and the gapped (semiconducting) phases. However, the possibility of Mottness in carbon-based materials [28] or in purely p-band [29] systems remains an open and intriguing problem since the naive expectation dictates that the itinerancy (kinetic energy of p carriers) is appreciable compared to the electron-electron interactions, which is distinct from d-band systems, where the d electrons reside in much narrower bands (hence, the effective U/W is sizable) [26]. Thus, searching for and characterizing Mott localization in systems with active p bands is an issue of contemporary and future interest.

II. RESULTS AND DISCUSSION

It is recognized that under external perturbations like lattice strain, the hopping elements are renormalized in nontrivial ways. On the other hand, due to its atomic nature the one-site Coulomb U interaction is expected to be less affected under extreme conditions. With this in mind, in this work we explore the effect of isotropic strain on the bare electronic structure of strained graphene [20], showing how it can be reshaped by interaction effects at not yet explored superstrained conditions. To establish that Mott localization can be naturally induced in two-dimensional graphene we carried out GGA+DMFT [24] calculations and investigated the reconstructed electronic properties of our superstrained graphene system. We focus mostly on correlation-induced Mott-Hubbard localization since the issue related to electronic reconstruction associated with the interplay between U and W at currently acceptable strain conditions [4] was already studied in Ref. [30]. However, if we aim to understand the material-specific properties, it is important to identify the character of dominant bands near the Fermi level and their energy distribution. For this purpose, the first-principles density functional theories (DFTs) are the best tools available. Hence, in Fig. 2 we show the GGA spectral function of natural graphene [31], i.e., with $L = 0.24669$ nm. At normal conditions, the sp^2 hybridization of atomic s-$p_{x,y}$ orbitals of carbon atoms create lateral σ bonds, and the remaining p_z orbital perpendicular to the plane forms the nonhybridized π bands in graphene and graphite. Due to strong in-plane covalency a large bonding-antibonding splitting is created in the planar (denoted as $p_{x,y}$) orbitals, resulting in a pronounced charge gap, as shown in Fig. 2. As seen in this figure, the electronic density of states (DOS) of the p_z orbital vanishes linearly near the Fermi energy at $E_F = \omega = 0$, exhibiting the semimetallic nature of graphene. As seen in Fig. 2, the linear (Dirac-like) band dispersion is reshaped by isotropically increasing the lattice constant L. An overall reduction of the one-electron bandwidth W, including the energy position of the van Hove singularities at the border of the Dirac dispersion, is found in the p_z band for the lattice constants varying from 0.24669 to 0.3209 nm [20,30]. Also interesting is the band structure reconstruction within the planar $p_{x,y}$ bands, where the charge gap shrinks with increasing lattice constant until it is fully suppressed at large L in GGA [20]. We notice here that even at larger C-C bond distances, the GGA forces acting between the carbon atoms are such that

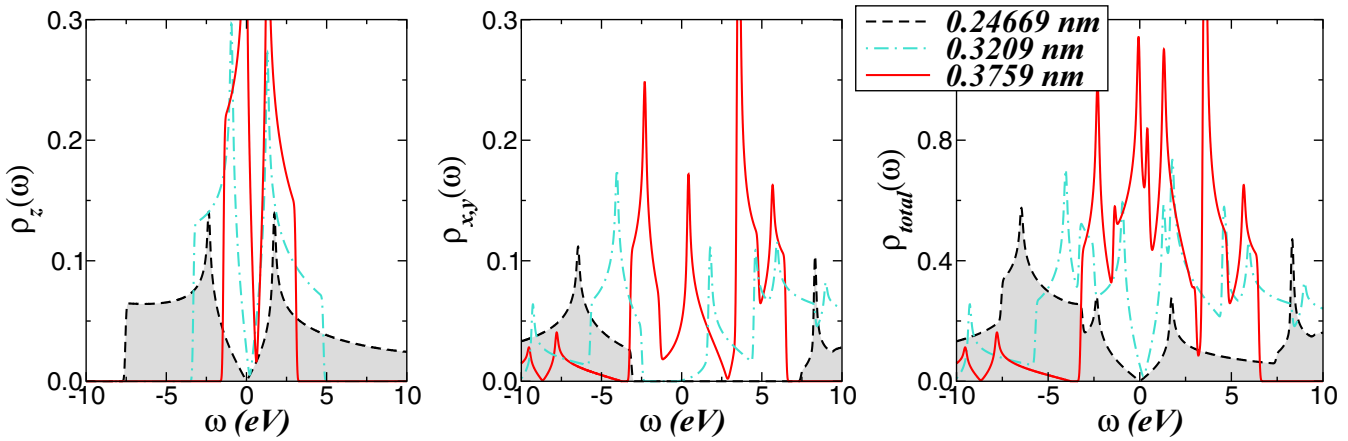

FIG. 2. GGA orbital-resolved and total DOS of graphene for different values of the lattice constant L. Notice the band narrowing and the evolution of the electronic spectrum with increasing L. A particularly relevant feature is the metallic state in GGA for $L = 0.3759$ nm. This corresponds to a C-C average bond length of 0.217 nm (0.142 nm in natural graphene).

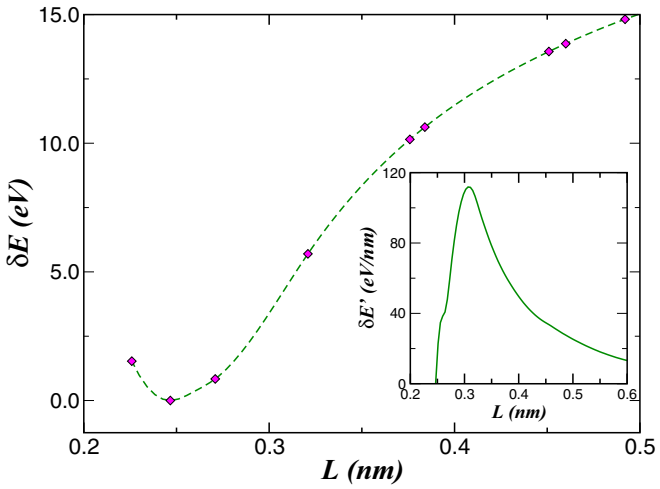

FIG. 3. Total energy difference $\delta E(L) \equiv E_L - E_{0.24669}$ between strained and natural graphene obtained from GGA calculations, showing the nonmonotonic response as a function of the lattice constant L. The inset shows the behavior of the external forces, $\delta E'(L) \equiv \frac{d}{dL}\delta E(L)$, required to stretch graphene. Notice the maximum in $\delta E'(L)$ for strain values around 25%, suggesting that a crossover between hard and soft graphene might be achieved in future experiments on superstrained graphene across the critical value $L_c = 0.309$ nm.

the equilibrium geometry is recovered upon release of the mechanical constraint. This in turn suggests accessibility of engineering a tunable bonded state in graphenelike systems. However, the central result seen in Fig. 2 is the pronounced one-particle band narrowing, which can be tuned by pulling the carbon atoms farther apart, in accordance with Mott ideas [27].

Within GGA we have also computed the total energy difference between strained (or compressed) and natural graphene [$\delta E \equiv E_L - E_{0.24669}$] as a function of the lattice constant L. As expected, our results in Fig. 3 show that the minimum value of δE is obtained for natural graphene, confirming the lattice stability of this fundamental $2D$ carbon allotrope. However, the fact that δE increases when $L \neq 0.24669$ nm naturally implies that graphene is resistant to strain or compressive strain. As visible in Fig. 3, the L dependence of δE is nonmonotonic with a tendency towards saturating behavior at extremely high lattice constant values (not shown). In order to explore the implications of our results for superstrained graphene, in the inset of Fig. 3 we display the forces [$\delta E'(L) \equiv \frac{d}{dL}\delta E$] needed to stretch graphene beyond its most stable configuration. Surprisingly, our results reveal a maximum in $\delta E'$ for a critical strain around 25%, a value close to that experimentally reported by Kim *et al.* [4]. This in turn implies that different elastic properties with a crossover between hard and soft graphene are expected to occur in monolayer graphene. According to our results in Fig. 3, above the critical value $L_c = 0.309$ nm strained graphene is predicted to lose its robust strength, and therefore, it will demand less work or effort to yield large symmetrical deformations. Our prediction is consistent with the electron localization function (ELF) [32] analysis in Fig. 4, where localization domains of the ELF around each carbon atom are clearly observed for $L = 0.3759$ nm [33]. Nevertheless, it might be plausible to assume that above L_c superstrained graphene might lose part of its intrinsic elasticity, being less capable of recovering its size and shape after strong deformations. Taken together, our *ab initio* GGA and ELF results in Figs. 3 and 4 strongly suggest that a defect-free graphene might support deformations well beyond the linear regime discussed in Ref. [17], and this prediction could be tested in future experiments on symmetrical superstrained graphene with strain values well above 30%.

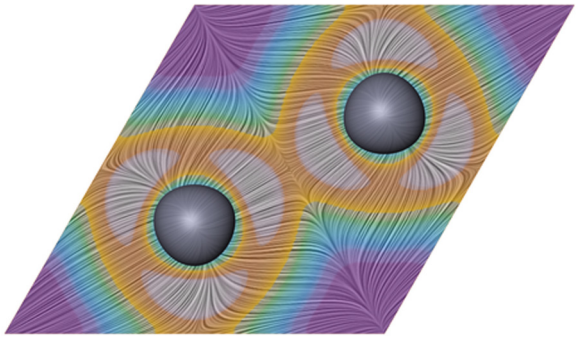

FIG. 4. Electron localization function (ELF) and electronic density gradient (gray field lines) analysis for symmetrical superstrained graphene with $L = 0.3759$ nm. Notice the C-C bond between the two carbon atoms. [The ELF color-map range used here goes from 0.0 (purple/black) to 1.0 (white)].

Multiorbital (MO) electron-electron interactions often drive spectacular effects in real materials: precisely how this might come about is an open, challenging problem also for wideband systems. Here, we study correlation-induced electronic reconstruction in superstrained graphene using combined GGA and DMFT methods. This scheme was used to revisit the long-standing issues of transport anisotropy due to incoherence-coherence crossovers in graphite [34] and to reveal the hidden correlated electronic structure of strained graphene with $L = 0.3209$ nm [30], both studies showing good agreement with spectroscopy (graphite) and tunneling (strained graphene nanobubbles) measurements. This gives us the confidence to use GGA+DMFT to predict the electronic properties of graphene at higher-lattice-strain conditions. The realistic Coulomb interaction parameter for natural graphene is $U = 9.3$ eV [25]. Owing to the metallic p-band DOS in strained graphene with $L = 0.3759$ nm (see Fig. 2), one expects the Hubbard U (or the on-site Coulomb interaction) to be partially screened compared to natural graphene. Thus, in our study we choose renormalized U values to reveal an interaction-induced Mott transition (which is characterized by a gap opening at E_F) for $L = 0.3759$ nm and realistic values of U.

The many-body Hamiltonian relevant for graphene [30] is $H = H_0 + H_{\rm int}$, with $H_0 = \sum_{\mathbf{k}a\sigma} \epsilon_a(\mathbf{k}) c^\dagger_{\mathbf{k}a\sigma} c_{\mathbf{k}a\sigma}$ and

$$H_{\rm int} = U \sum_{ia} n_{ia\uparrow} n_{ia\downarrow} + \sum_{ia\neq b} U' n_{ia} n_{ib} - J_H \sum_{ia\neq b} \mathbf{S}_{ia} \cdot \mathbf{S}_{ib}.$$

Here, $a = x,y,z$ label the diagonalized p bands, and $\epsilon_a(\mathbf{k})$ is the one-electron band dispersion, which encodes details of the one-electron (GGA) band structure. $U' \equiv U - 2J_H$, with U, U' being the intra- and interorbital Coulomb repulsions

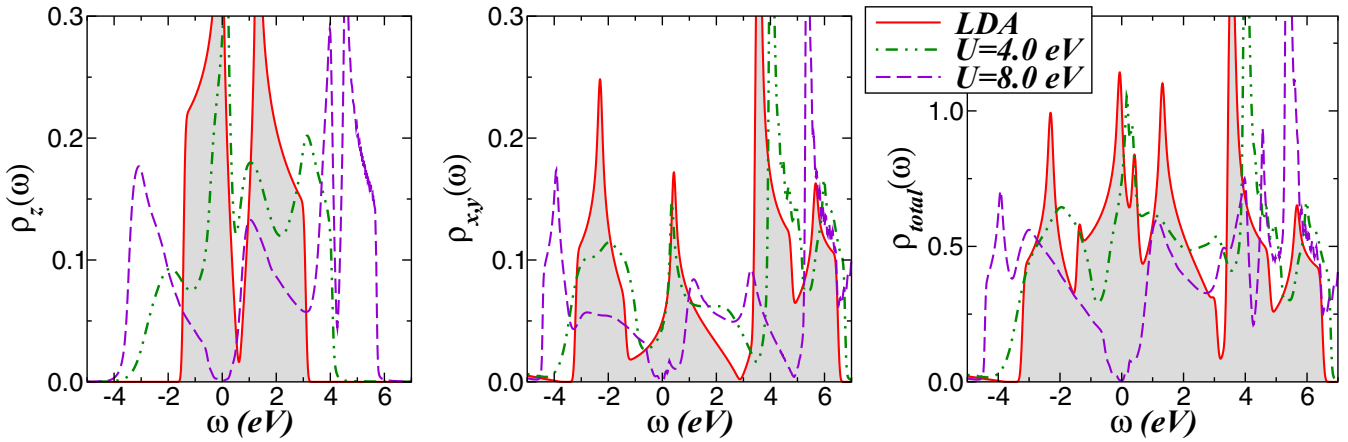

FIG. 5. Comparison between GGA (solid line) and GGA+DMFT results of (super)strained graphene with $L = 0.3759$ nm. Notice the evolution towards a Mott insulator with increasing on-site Coulomb repulsion U. Compared to the GGA results, large spectral weight transfer is visible in the GGA+DMFT spectral functions.

and J_H being Hund's rule coupling. The effect of tuning the one-band dispersions is read off from $\epsilon_a(\mathbf{k})$: these are inputs for MO DMFT, which generates a Mott insulating state for $U = 6.1$ eV at $L = 0.3759$ nm, as shown below. We use MO DMFT for the three-orbital model of strained graphene with the MO iterated perturbation theory (MO-IPT) as the impurity solver. The detailed formulation of MO-IPT for correlated electron systems has already been developed [35] and used in the context of carbon-based systems in Refs. [30,34,36], so we do not repeat the equations here.

To pinpoint the excitation spectrum that emerges from dynamical MO electron-electron interactions in superstrained graphene (with $L = 0.3759$ nm chosen), we present in Fig. 5 our GGA+DMFT results for $U = 4.0$ and 8 eV with fixed $J_H = 0.4$ eV. (Our choice for J_H is in accordance with values estimated within GGA on a different local moment problem in graphene [37].) The formation of the Mott-Hubbard insulating gap at low energies with the concomitant appearance of lower (LHB) and upper (UHB) Hubbard bands on different orbitals at high energies with increasing U is visible in Fig. 5. As common in a system approaching the Mott transition, electron-electron interactions strongly modify the bare GGA spectral functions. MO dynamical correlations arising from U, U' and J_H lead to spectral weight redistribution over large energy scales and the formation of LHB (local moments) and UHB at high energies. Noticeable differences in the spectral weight transfer (SWT) are seen between the p_z and $p_{x,y}$ channels. Within the p_z orbital the LHB at $\omega \approx 2.0$ eV for $U = 4$ eV (and $U' = 3.2$ eV) is clearly resolved and moves to higher energies with increasing U. SWT is also seen within the planar orbitals. Interestingly, in these channels the bonding-antibonding bands in GGA are transferred to higher energies, but their spectral line shape remains close to that found in GGA, indicating that dynamical correlations partially renormalize the C-C bonds. Hence, as in transition-metal systems under extreme conditions [26], it is plausible to assume that the Mott phase

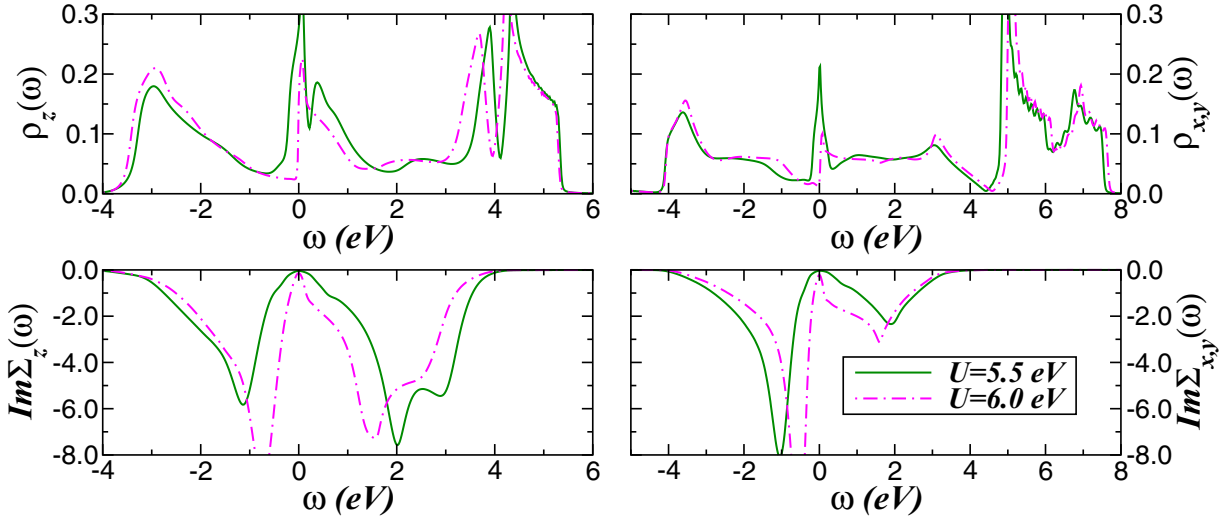

FIG. 6. Orbital-resolved spectral functions and imaginary parts of the self-energies of superstrained graphene for two values of U and $J_H = 0.4$ eV. A crossover from a selective-Kondo ($U = 5.5$ eV) to an incoherent metallic regime (at $U = 6.0$ eV) is visible. Notice the evolution of the self-energies near E_F across the correlation-induced Fermi to non-Fermi liquid crossover.

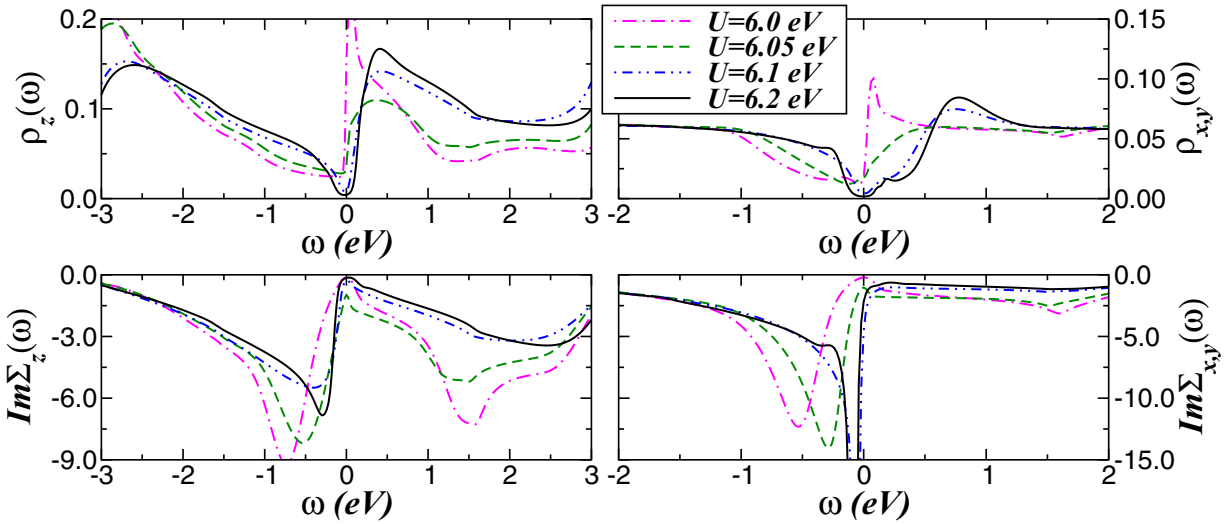

FIG. 7. Orbital-resolved GGA+DMFT DOS and imaginary parts of the self-energies of superstrained graphene near the Mott transition point at 6.05 eV $\leqslant U_c \leqslant$ 6.1 eV. Notice the sharp pole in the planar $p_{x,y}$ self-energies near E_F within the Mott insulating phase of graphene at extreme strain conditions. This behavior is characteristic of selective Mott physics in multiorbital systems.

sets in without spontaneously breaking the hexagonal crystal lattice of our superstrained graphene.

Since the dependence of electron-electron interactions in the excitation-spectrum graphene-based systems is quite subtle and not yet fully understood [38], in Fig. 6 we display the orbital-resolved DOS and the imaginary part of self-energies $\mathrm{Im}\Sigma_a(\omega)$ within the correlated metal phase. Up to $U = 5.0$ eV the charge carriers of highly strained graphene are in a Fermi liquid (FL) regime, characterized by the emergence of narrow quasiparticle resonances in the orbital-selective DOS near E_F and ω^2 dependence in the self-energy imaginary parts (see Fig. 6). Moreover, as can be seen in Fig. 6, our self-consistent GGA+DMFT calculation also resolves a pseudogap feature near E_F for $U = 6.0$ eV, implying a crossover from a FL to a non-FL regime. This behavior is often seen in MO metallic systems close to Mottness, where strong orbital and spin fluctuations prevent the FL fixed point. In our superstrained graphene system the transfer of spectral weight found in the FL and non-FL metallic phases can be traced to a dynamical scattering process that leads to electron mass enhancement, which is not expected for massless Dirac fermion systems like in natural graphene [39].

To further illustrate the correlated nature of our spectral functions near the localization-delocalization transition point, in Fig. 7 we show the changes in the orbital-resolved DOS and $\mathrm{Im}\Sigma_a(\omega)$ across the Mott transition. Interestingly, the transition found here is of first-order type showing large-scale changes in SWT at the (6.05 eV $< U_c <$ 6.1 eV) phase boundary. In this regime, the imaginary parts of the orbital-resolved self-energies in Fig. 7 display signatures of selective Mott-Hubbard physics. The out-of-plane p_z orbital shows weak deviations from the $-\omega^2$ (FL) form at small ω, being consistent instead with a sublinear ω dependence, along with a finite value at $E_F(\omega = 0)$ for $U = 6.05$ eV. On the other hand, the $p_{x,y}$ self-energies reveal strong Mott localization physics. The Mott-Hubbard insulating state thus goes hand in hand with the development of a sharp pole in $\mathrm{Im}\Sigma_{x,y}(\omega)$ close to E_F. This implies that the charge carriers in superstrained graphene have a dual nature, where effectively Mott localized $p_{x,y}$ states coexist with incoherent p_z electronic states at $U = 6.1$ eV. In this two-fluid scenario localization of the $p_{x,y}$ states in our system implies that these orbitals now act like an intrinsic source of electronic disorder in the system. With $U' = 5.3$ eV this suggests that an intrinsic disorder potential, arising from orbital-selective physics, exists near the Mott transition. Such behavior results from strong scattering between effectively (Mott) localized and quasiitinerant components of the full DMFT matrix propagators. Our work calls for electrical transport studies in superstrained graphene. These studies will constitute a proof to Mott localization and the ability of defect-free graphene to afford large strain deformation as well as the importance of treating dynamical correlations adequately to reveal a variety of unexplored responses in complex materials.

III. CONCLUSION

In conclusion, we have performed first-principles GGA calculations to confirm that semimetal graphene turns to metallic when increasing the lattice constant from 0.24669 to 0.3759 nm [20]. Using GGA+DMFT for a realistic multi-orbital Hubbard model, we explore the correlated nature of the excitation spectrum of a superstrained graphene. In a regime of isotropically large lattice distances, the interplay between one-particle band narrowing and multiorbital electron-electron interactions pushes strained graphene into a Mott insulating state characterized by selective orbital physics at low energies. Our microscopic description of coupled multiorbital Hubbard interactions is expected to be generally applicable to three-dimensional flexible graphene networks [23] as well as for superstrechable graphene films for transparent and biocompatible electrodes [4,5].

ACKNOWLEDGMENTS

L.C. is supported by CNPq (Grant No. 307487/2014-8). L.C. also thanks the Theoretical Chemistry Department at Technical University Dresden for hospitality. S.L. thanks the DFG for support under the priority project SPP 1415 and for a personal Heisenberg grant.

[1] A. H. Castro Neto, F. Guinea, N. M. R. Peres, K. S. Novoselov, and A. K. Geim, Rev. Mod. Phys. **81**, 109 (2009).

[2] D. R. Cooper, B. D'Anjou, N. Ghattamaneni, B. Harack, M. Hilke, A. Horth, N. Majlis, M. Massicotte, L. Vandsburger, E. Whiteway, and V. Yu, arXiv:1110.6557.

[3] Y. Wu, Y.-M. Lin, A. A. Bol, K. A. Jenkins, F. Xia, D. B. Farmer, Y. Zhu, and P. Avouris, Nature (London) **472**, 74 (2011); Y.-M. Lin, C. Dimitrakopoulos, K. A. Jenkins, D. B. Farmer, H.-Y. Chiu, A. Grill, and Ph. Avouris, Science **327**, 662 (2010).

[4] K. S. Kim, Y. Zhao, H. Jang, S. Y. Lee, J. M. Kim, K. S. Kim, J.-H. Ahn, P. Kim, J.-Y. Choi, and B. H. Hong, Nature (London) **457**, 706 (2009).

[5] C. F. Guo, Q. Liu, G. Wang, Y. Wang, Z. Shi, Z. Suo, C.-W. Chu, and Z. Ren, Proc. Natl. Acad. Sci. U.S.A. **112**, 12332 (2015).

[6] D. Pesin and A. H. MacDonald, Nat. Mater. **11**, 409 (2012).

[7] J. Nilsson, A. H. Castro Neto, F. Guinea, and N. M. R. Peres, Phys. Rev. B **76**, 165416 (2007).

[8] J. Yun, Y. Lim, G. N. Jang, D. Kim, S. J. Lee, H. Park, S. Y. Hong, G. Lee, G. Zi, and J. S. Ha, Nano Energy **19**, 401 (2016).

[9] A. A. Balandin, Nat. Mater. **10**, 569 (2011); C. Berger, Z. Song, X. Li, X. Wu, N. Brown, C. Naud, D. Mayou, T. Li, J. Hass, A. N. Marchenkov, E. H. Conrad, P. N. First, and W. A. de Heer, Science **312**, 1191 (2006).

[10] S. Y. Zhou, G.-H. Gweon, A. V. Fedorov, P. N. First, W. A. de Heer, D.-H. Lee, F. Guinea, A. H. Castro Neto, and A. Lanzara, Nat. Mater. **6**, 770 (2007).

[11] S. Y. Zhou, D. A. Siegel, A. V. Fedorov, and A. Lanzara, Phys. Rev. Lett. **101**, 086402 (2008).

[12] R. M. Ribeiro, N. M. R. Peres, J. Coutinho, and P. R. Briddon, Phys. Rev. B **78**, 075442 (2008).

[13] S. S. Carara, R. J. C. Batista, and H. Chacham, Phys. Rev. B **80**, 115435 (2009).

[14] G. Giovannetti, P. A. Khomyakov, G. Brocks, P. J. Kelly, and J. van den Brink, Phys. Rev. B **76**, 073103 (2007).

[15] Z. H. Ni, T. Yu, Y. H. Lu, Y. Y. Wang, Y. P. Feng, and Z. X. Shen, ACS Nano **2**, 2301 (2008).

[16] N. N. Klimov, S. Jung, S. Zhu, T. Li, C. A. Wright, S. D. Solares, D. B. Newell, N. B. Zhitenev, and J. A. Stroscio, Science **336**, 1557 (2012); T. M. G. Mohiuddin, A. Lombardo, R. R. Nair, A. Bonetti, G. Savini, R. Jalil, N. Bonini, D. M. Basko, C. Galiotis, N. Marzari, K. S. Novoselov, A. K. Geim, and A. C. Ferrari, Phys. Rev. B **79**, 205433 (2009).

[17] C. Lee, X. Wei, J. W. Kysar, and J. Hone, Science **321**, 385 (2008).

[18] M. L. Teague, A. P. Lai, J. Velasco, C. R. Hughes, A. D. Beyer, M. W. Bockrath, C. N. Lau, and N.-C. Yeh, Nano Lett. **9**, 2542 (2009); N. Ferralis, R. Maboudian, and C. Carraro, Phys. Rev. Lett. **101**, 156801 (2008).

[19] V. M. Pereira and A. H. Castro Neto, Phys. Rev. Lett. **103**, 046801 (2009); F. M. D. Pellegrino, G. G. N. Angilella, and R. Pucci, Phys. Rev. B **84**, 195404 (2011); **81**, 035411 (2010).

[20] G. Gui, J. Li, and J. Zhong, Phys. Rev. B **78**, 075435 (2008).

[21] M. Farjam and H. Rafii-Tabar, Phys. Rev. B **80**, 167401 (2009).

[22] D. J. Lipomi, M. Vosgueritchian, B. C.-K. Tee, S. L. Hellstrom, J. A. Lee, C. H. Fox, and Z. Bao, Nat. Nanotechnol. **6**, 788 (2011).

[23] Z. Chen, W. Ren, L. Gao, B. Liu, S. Pei, and H.-M. Cheng, Nat. Mater. **10**, 424 (2011).

[24] G. Kotliar, S. Y. Savrasov, K. Haule, V. S. Oudovenko, O. Parcollet, and C. A. Marianetti, Rev. Mod. Phys. **78**, 865 (2006).

[25] T. O. Wehling, E. Şaşıoğlu, C. Friedrich, A. I. Lichtenstein, M. I. Katsnelson, and S. Blügel, Phys. Rev. Lett. **106**, 236805 (2011).

[26] M. Imada, A. Fujimori, and Y. Tokura, Rev. Mod. Phys. **70**, 1039 (1998).

[27] N. F. Mott, *Metal-Insulator Transitions* (Taylor and Francis, London, 1974).

[28] P. Durand, G. R. Darling, Y. Dubitsky, A. Zaopo, and M. J. Rosseinsky, Nat. Mater. **2**, 605 (2003).

[29] J. A. Chan, S. Lany, and A. Zunger, Phys. Rev. Lett. **103**, 016404 (2009); J. Winterlik, G. H. Fecher, C. A. Jenkins, C. Felser, C. Mühle, K. Doll, M. Jansen, L. M. Sandratskii, and J. Kübler, *ibid.* **102**, 016401 (2009); A. J. R. da Silva and L. M. Falicov, Phys. Rev. B **52**, 2325 (1995).

[30] L. Craco, D. Selli, G. Seifert, and S. Leoni, Phys. Rev. B **91**, 205120 (2015).

[31] Here, the optimum geometry and stability of the system were investigated within density functional theory, as implemented in the SIESTA simulation package [40]. We used generalized gradient approximation with the Perdew-Burke-Ernzerhof [41] exchange-correlation functional with norm-conserving Troullier-Martins pseudopotentials [42]. The charge density was represented on a real-space grid with an energy cutoff of 200 Ry. The reciprocal space was sampled with a fine $180 \times 1 \times 180$ Monkhorst-Pack k-point grid [43].

[32] S. Leoni, L. Craco, A. Ormeci, and H. Rosner, Solid State Sci. **8**, 1138 (2006).

[33] See also Ref. [20] for a detailed chemical bonding analysis based on ELF of strained and compressed graphene with different lattice deformation conditions.

[34] L. Craco, M. S. Laad, S. Leoni, and A. S. de Arruda, Phys. Rev. B **87**, 155109 (2013).

[35] L. Craco, Phys. Rev. B **77**, 125122 (2008).

[36] L. Craco, S. S. Carara, T. A. da Silva Pereira, and M. V. Milošević, Phys. Rev. B **93**, 155417 (2016).

[37] M. Casartelli, S. Casolo, G. F. Tantardini, and R. Martinazzo, Phys. Rev. B **88**, 195424 (2013).

[38] V. N. Kotov, B. Uchoa, V. M. Pereira, F. Guinea, and A. H. Castro Neto, Rev. Mod. Phys. **84**, 1067 (2012); H.-K. Tang, E. Laksono, J. N. B. Rodrigues, P. Sengupta, F. F. Assaad, and S. Adam, Phys. Rev. Lett. **115**, 186602 (2015).

[39] K. S. Novoselov, A. K. Geim, S. V. Morozov, D. Jiang, M. I. Katsnelson, I. V. Grigorieva, S. V. Dubonos, and A. A. Firsov, Nature (London) **438**, 197 (2005).

[40] J. M. Soler, E. Artacho, J. D. Gale, A. García, J. Junquera, P. Ordejón, and D. Sánchez-Portal, J. Phys. Condens. Matter **14**, 2745 (2002).

[41] J. P. Perdew, K. Burke, and M. Ernzerhof, Phys. Rev. Lett. **77**, 3865 (1996).

[42] N. Troullier and J. L. Martins, Phys. Rev. B **43**, 8861 (1991).

[43] H. J. Monkhorst and J. D. Pack, Phys. Rev. B **13**, 5188 (1976).